

Uranium Uptake from Aqueous Solution by Interaction with Goethite, Lepidocrocite, Muscovite, and Mackinawite: An X-ray Absorption Spectroscopy Study

LESLEY N MOYES,* †
 RICHARD H PARKMAN,† ‡
 JOHN M CHARNOCK,† † §
 DAVID J VAUGHAN,†
 FRANCIS R LIVENS,†
 COLIN R HUGHES,† AND
 ANNA BRAITHWAITE^{||}

Department of Chemistry and Department of Earth Sciences
 University of Manchester, Manchester M13 9PL, U K,
 CLRC Daresbury Synchrotron Laboratory,
 Warrington, WA4 4AD, U K, and BNFL plc,
 Sellafield, Seascale, Cumbria, CA20 1PG, U K

The retention of radionuclides by interaction with mineral phases has significant consequences for the planning of their short- and long-term disposal to geological systems. An understanding of binding mechanisms is important in determining the ultimate fate of radionuclides following release into natural systems and will give increased confidence in predictive models. X-ray absorption spectroscopy (XAS) has been used to study the local environment of uranium taken up from aqueous solution by the surfaces of goethite, lepidocrocite, muscovite, and mackinawite. On both iron hydroxides uranium uptake occurs by surface complexation and ceases when the surface is saturated. The muscovite surface does not become saturated and uptake increases linearly suggesting formation of a uranyl phase on the surface. Uranium uptake on mackinawite also suggests a replacement or precipitation process. XAS indicates that bidentate inner-sphere surface complexes are formed on the iron hydroxides by coordination of two surface oxygens from an iron octahedron in the equatorial plane of the complex. Uranium uptake on muscovite may occur through surface precipitation, the first layer of uranium atoms binding through equatorial coordination of two adjacent surface oxygens from a silicate tetrahedron, with the axial oxygens of the uranyl unit aligned across the hexagonal "cavities" created by the rings of tetrahedra. At low concentrations, uptake on mackinawite occurs at locally oxidized regions on the surface via a similar mechanism to that on iron hydroxides. At the highest concentrations, equatorial oxygen bond distances around 2.0–2.1 Å are observed, inconsistent with the presence of uranyl species. The average number of axial oxygens also decreases with increasing concentration, and these results suggest partial reduction of uranium. The nature of these different surface reactions plays an important role in assessing the geochemical behavior of uranium in natural systems, particularly under reducing conditions.

Introduction

The uptake of uranium on soil and sediment components has been extensively studied (1–11). Many of these studies have been concerned with the binding mechanisms of the uranyl ion (UO_2^{2+}) under oxic conditions.

Morris et al. (7) used Raman spectroscopy to identify distinct binding sites on a smectite clay. At low and intermediate loadings of uranium, uptake occurs at pH-dependent amphoteric edge sites, and, at higher loadings, binding occurs at fixed charge (exchange) surface sites. Further studies on clay minerals have shown that as surface coverage increases, the number of equatorial oxygens around the uranyl unit increases, as does the U–O bond distance (6). This suggests that initial uptake to the most energetically favorable sites allows a close approach of the uranyl unit and an inner-sphere reaction with the surface. After this, uptake is on to less favorable sites, so that the U–O distance increases with uptake. At high surface coverage, the binding complex appears to be similar to that in the aqueous phase, implying unselective and weak binding.

Uranium binding by iron oxide minerals also appears to be by inner-sphere surface complex formation involving two oxygens of the FeO_6 octahedron (8). Surface complexation modeling of uranyl species in carbonate-free solution at pH > 5 suggests that mono-, bi-, and tridentate uranyl-hydroxy complexes are responsible for uptake on ferric hydroxides (2). Uranium uptake on calcite is a complex combination of processes depending on pH and on CO_2 and U concentrations, under some conditions uranium is weakly adsorbed as a monolayer, while under others formation of a precipitate on the calcite surface is observed (12). Sulfide minerals also take up uranium (5, 13, 14), and reduction of trace metals in solution by sulfide minerals has been observed (9, 15).

Uptake studies which rely on bulk measurements (sorption isotherms, distribution coefficients) are essential to understand the behavior of uranium under different pH, temperature, and concentration conditions. However, to give increased confidence, they need to be combined with direct observation of species coordination at the mineral/water interface. X-ray absorption spectroscopy (XAS) is the most effective way of analyzing the local environment of uranium species bound to a fine particle mineral phase and has the ability to distinguish between various adsorption and surface precipitation processes (16). For these reasons, this study concentrates on the XAS analysis of uranium taken up on several mineral phases and compares the different coordination behavior observed. The current work supports and extends previously reported experiments on iron oxides/hydroxides under a variety of conditions (1, 2, 8) and reports, for comparison, new studies involving muscovite and mackinawite.

Experimental Section

In this work, powdered samples of the mineral phases were reacted with solutions of the uranyl ion (as nitrate) at increasing concentrations, and the uranium uptake measured. The form in which the uranium was taken up by each mineral was then investigated using X-ray absorption spectroscopy.

* Corresponding author phone +44(161) 275 4647 fax +44(161) 275-4598 e mail Lesley.Moyes@man.ac.uk

† Department of Chemistry, University of Manchester

‡ Department of Earth Sciences University of Manchester

§ CLRC Daresbury Synchrotron Laboratory

^{||} BNFL plc Sellafield Seascale Cumbria CA20 1PG U K

ADMIN RECORD

13

Mineral Preparation Goethite and lepidocrocite were synthesized according to Schwertmann and Cornell (17), and the purity and homogeneity were confirmed by powder X-ray diffraction (XRD). Goethite and lepidocrocite prepared by this method typically have surface areas of 20 and 70–80 m² g⁻¹, respectively. A natural muscovite sample was ground with acetone in a planetary ball mill. The surface area (BET isotherm method) of the powdered material was 39.8 m² g⁻¹. Mackinawite (tetragonal FeS_{1-x}) was obtained by precipitation from an aqueous Fe(II) solution by addition of aqueous Na₂S at controlled pH, as described by Lennie et al. (18) and Lennie and Vaughan (19). This procedure was carried out using deaerated deionized water under an oxygen-free nitrogen atmosphere. The freeze-dried precipitate was stored under nitrogen. The sample was amorphous when examined by X-ray powder diffraction, however, extended absorption fine structure spectroscopy (EXAFS) analysis of the Fe K-edge gave coordination numbers and interatomic distances (four S atoms at 2.20 Å and four Fe atoms at 2.5–2.6 Å) consistent with mackinawite as described by Lennie et al. (18) and Lennie and Vaughan (19). The material is prone to oxidation, making surface area measurements difficult.

Batch Experiments In the batch uptake experiments, a solid/solution ratio of 0.1 g/10 mL was used for the goethite and mackinawite, while 0.3 g/30 mL was used for the lepidocrocite and muscovite. With the exception of mackinawite (see below), the samples of solid material were rewet overnight in deionized water (10 or 30 mL as appropriate) in 50 mL capped polyethylene centrifuge tubes. Uranyl nitrate in aqueous solution was added to give initial uranium solution concentrations of 0.025, 0.05, 0.1, 0.2, 0.5, and 1.0 mM. Spike volumes did not exceed 100 µL, to avoid significantly affecting the solid/solution ratio. In all cases, three identical samples were prepared for each concentration. The uranium solution was kept in contact with the solid material for 24 h and agitated. Final pH values were 3.6–4.8 for lepidocrocite, 3.7 (high [U]_{soln}) – 7.0 (low [U]_{soln}) for goethite, and 4.6 (high [U]_{soln}) – 8.1 (low [U]_{soln}) for muscovite. The implications of these variations in pH are discussed later. After centrifuging (6000 rpm, 30 min), the supernatants were removed and filtered (0.45 µm), and a known aliquot was diluted appropriately with 2% (v/v) HNO₃ (Aristar) for analysis by inductively coupled plasma mass spectrometry (ICPMS). The remaining slurry of solid material was sealed in the centrifuge tube and frozen in liquid nitrogen to minimize further reaction before X-ray absorption analysis.

The mackinawite samples were treated similarly, except all manipulations were carried out in a glovebag under an oxygen-free nitrogen atmosphere and using degassed deionized water. Initial solution concentrations ranged from 0.5 to 5.0 mM. The remaining slurry was carefully inserted into polyethylene tubing (ca. 5 mm diameter), sealed, and frozen in liquid nitrogen. At all concentrations of uranium in solution the pH equilibrated between pH 6.7 and 7.0, suggesting that addition of the uranium did not significantly affect the pH of the system.

X-ray Absorption Spectroscopy The local environment of the uranium taken up by the solid minerals was investigated by both X-ray absorption near edge structure (XANES) and extended X-ray absorption fine structure (EXAFS) spectroscopies. The general principles of XAS and its applications to mineral systems have been comprehensively reviewed elsewhere (20, 21).

Uranium L(III)-edge X-ray absorption spectra were collected on Station 9.2 at the CLRC Daresbury Synchrotron Radiation Source, operating at 2 GeV with a typical beam current of 150 mA. A double crystal Si (220) monochromator was used and detuned to 50% of maximum intensity to minimize high energy harmonic contamination. A frozen slurry sample, prepared as described above, was mounted

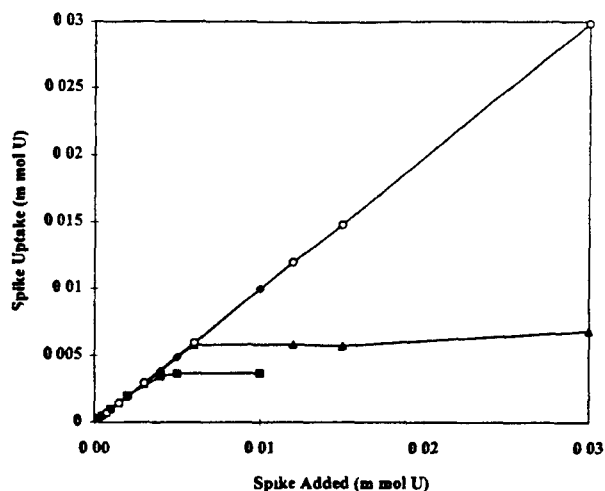


FIGURE 1 Uptake of uranium from solution as a function of initial uranium solution concentration (▲) on lepidocrocite, (■) on goethite, (○) on muscovite, and (◇) on mackinawite

in an aluminum sample holder and kept at liquid nitrogen temperature. The monochromator was calibrated using a crystalline UO₃ standard sample (edge position 17 169 eV). Fluorescence spectra were collected over an energy range of ~16 900 eV to ~18 050 eV using a 13-element Ge detector. The signal from each element was collected and examined separately before being added to the total. A minimum of four scans per sample were collected, and the data summed to improve data quality. An aqueous solution of uranyl nitrate (50 mM) and solid samples of U₃O₈ and UO₂ (diluted with boron nitride) were also analyzed. Background subtracted spectra were analyzed in EXCURV97 (22) using full curved wave theory, including multiple scattering from the uranyl group where necessary (23–25). Phase shifts were derived in the programs from ab initio calculations using Hedlin-Lundqvist potentials and von Barth ground states (26). Fourier transforms of the EXAFS spectra were used to obtain an approximate radial distribution function around the central uranium atom (the absorber atom), the peaks of the Fourier transform can be related to “shells” of surrounding backscattering atoms characterized by atom type, number of atoms in the shell, the absorber-scatterer distance, and a Debye-Waller factor, 2σ² (a measure of both the thermal disorder or range of absorber-scatterer distances, which may be viewed as an index of uncertainty in an individual shell). The data were fitted for each sample by defining a theoretical model and comparing the calculated EXAFS spectrum with the experimental data. Shells of backscatterers were added around the uranium and by refining an energy correction E_f (the Fermi energy), the absorber-scatterer distance, and the Debye-Waller factor for each shell, a least squares residual (the R factor (27)) was minimized. For each shell of scatterers around the uranium, the number of atoms in the shell was chosen to give the best fit but not refined. Additional shells of scatterers beyond the first were only included in the final fit if they made an improvement in the R-factor (at least 4%). Multiple scattering was included in the theoretical model, where necessary, by defining the geometry of the model and calculating all the multiple scattering pathways during refinement, using small atom theory (28) to minimize computation time.

Results and Discussion

Batch Experiments The uptake of uranium as a function of initial solution concentration is shown for each of the minerals in Figure 1, although it is difficult to interpret these

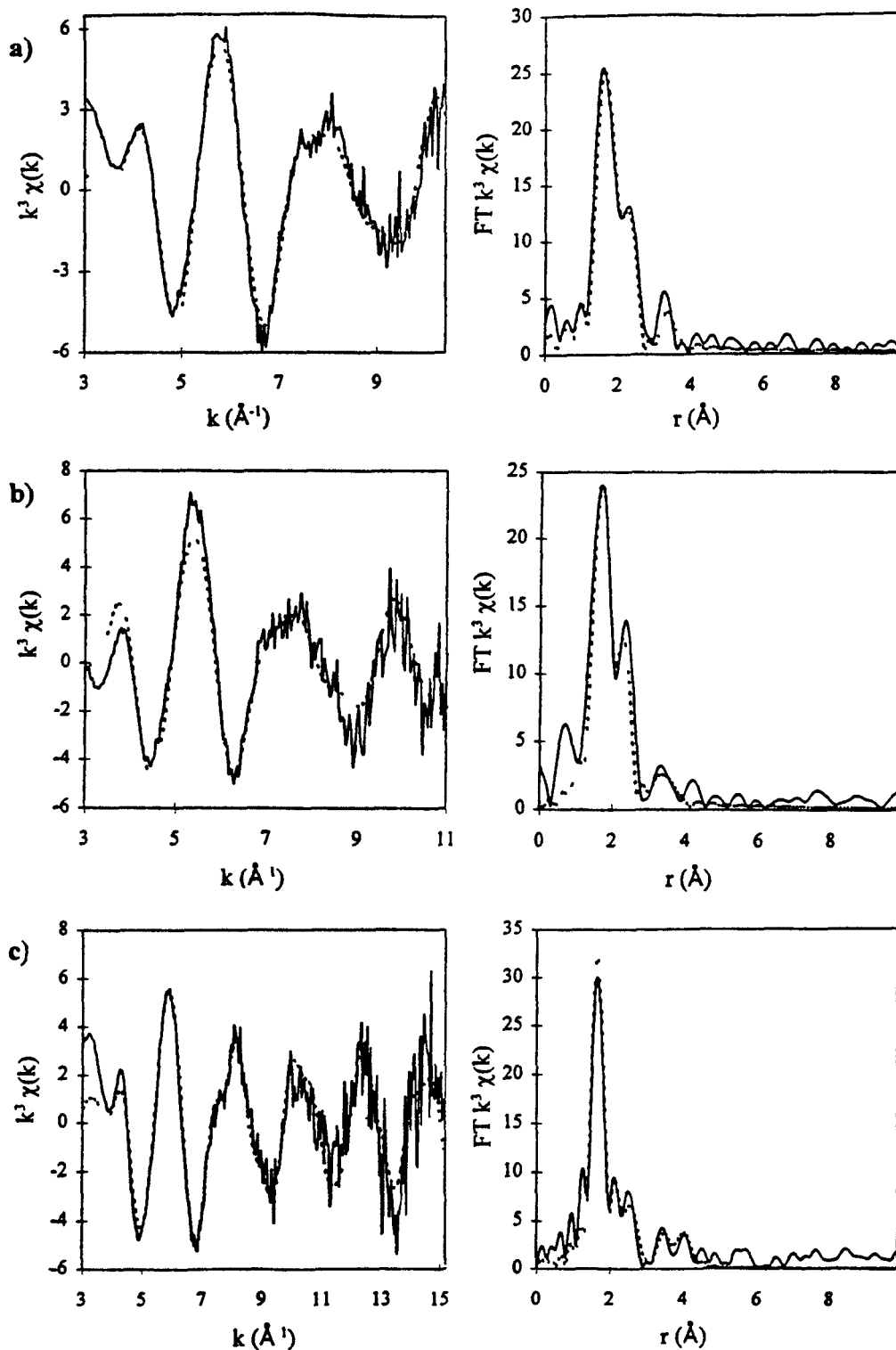


FIGURE 2. k^2 -weighted EXAFS and Fourier transforms for U on (a) lepidocrocite (from 0.5 mM U solution), (b) goethite (from 0.2 mM U solution), and (c) muscovite (from 0.4 mM U solution). Solid lines represent experimental data and dashed lines the best fit.

in detail due to the variability in pH. However, at the pH conditions employed uranyl hydroxy solution species are dominant in all systems (1, 29). Uptake on lepidocrocite and goethite follow very similar patterns, flattening off at higher concentrations. Uranium solution concentration has been shown to have a significant effect on sorption energetics (6, 7, 30), and these results indicate saturation of the available surface sites in support of previous work (3, 31). Uptake of uranium on muscovite and mackinawite is very different, increasing linearly with concentration and exceeding 99% at

each concentration. In effect, uranium is quantitatively removed from solution at all concentrations. In the case of muscovite, the surface loadings greatly exceed the cation exchange capacity of 18.8 ± 3.4 cmol/kg. This behavior suggests formation of a new phase at the surface (32). The continued uptake of uranium with increasing concentration on both muscovite and mackinawite may be due to the formation of a new uranium-containing phase on the surface. This hypothesis is examined in more detail in the following sections.

TABLE 1 Parameters Obtained from EXAFS Data Fitting of U L(III)-Edge Spectra for Lepidocrocite, Goethite, and Muscovite^a

sample (initial soln concn)	shell no	atom type	N	r(Å)	2σ ² (Å ²)	R
U on lepidocrocite (0.5 mM)	1	O	2.0	1.81	0.003	25.9
	2	O	4.0	2.40	0.015	
	3	Fe	1.0	3.45	0.017	
U on goethite (0.2 mM)	1	O	2.0	1.80	0.006	38.9
	2	O	5.0	2.40	0.024	
	3	Fe	1.0	3.47	0.015	
U on muscovite (0.4 mM)	1	O	2.0	1.80	0.003	40.1
	2	O	4.0	2.35	0.028	
	3	Si	1.0	2.75	0.011	
	4	Si	2.0	3.66	0.010	
	5	U	1.0	3.86	0.010	

^a N is the coordination number (±1) r is the interatomic distance (±0.02 Å) 2σ² is the Debye-Waller factor and R is the overall goodness of fit

Analysis of EXAFS Spectra. For lepidocrocite, goethite, and muscovite all the XAS spectra were very similar, regardless of uranium concentration. The results for one representative sample of each of these are therefore discussed in detail. The EXAFS spectra and corresponding Fourier transforms for these samples are shown in Figure 2a-c. Corresponding parameters obtained from analysis of the spectra are summarized in Table 1.

U on Fe Hydroxides. For both lepidocrocite and goethite (Figure 2a,b), the best fit was achieved with two axial uranyl oxygens at ~1.80 Å and five oxygen atoms at ~2.40 Å. These distances suggest uptake of the uranyl ion, coordinated in the equatorial plane by 4-6 ligands. In each case the fit is improved by a third shell containing at least one Fe atom at ~3.50 Å. This is also consistent with results of Waite et al (8), whose study of uranyl ion uptake on ferrihydrite surfaces also suggested that the equatorial oxygens could be separated into two groups, with 3 O at 2.35 Å and 2 O at 2.52 Å. In the present study, the resolution of the data was such that no improvement in fit was found on fitting with the equatorial oxygens as two shells. Uranyl carbonate complexes have been proposed on iron oxide surfaces from XAS analysis (33), but attempts to fit our data with carbonate ligands gave no improvement in fit.

Our EXAFS data suggest one environment for the equatorial oxygens. However, as Waite et al (8) proposed there may be more than one type of equatorial U-O environment, with the U-O distances to the surface O atoms being longer than those to the water ligands. If this is the case, then for the U-Fe distance obtained experimentally in our work, the distance between U and surface O would have to be ~2.50 Å, close to that found by Waite et al (8). If the equatorial oxygens are at two distinct distances, then given the experimental average equatorial U-O distance of ~2.40 Å, the remaining three equatorial O atoms would be at 2.33 Å which is very similar to the distance observed by Waite et al (8).

U on Muscovite. In common with the results for U on the iron hydroxides, the best fit to the EXAFS data for U on muscovite (Figure 2c) also shows two uranyl oxygens at 1.80 Å and at least four equatorial oxygen ligands at a shorter distance of 2.35 Å. Fitting the equatorial oxygens at two different distances did not improve the fit, but the high Debye-Waller factor (Table 1) may signify slight differences in U-O distances in the second shell. An improved fit is obtained when silicon atoms are fitted in third and fourth shells with a best model fit obtained with one silicon at 2.75 Å and two at 3.66 Å. However, a U-Si distance of 2.75 Å is

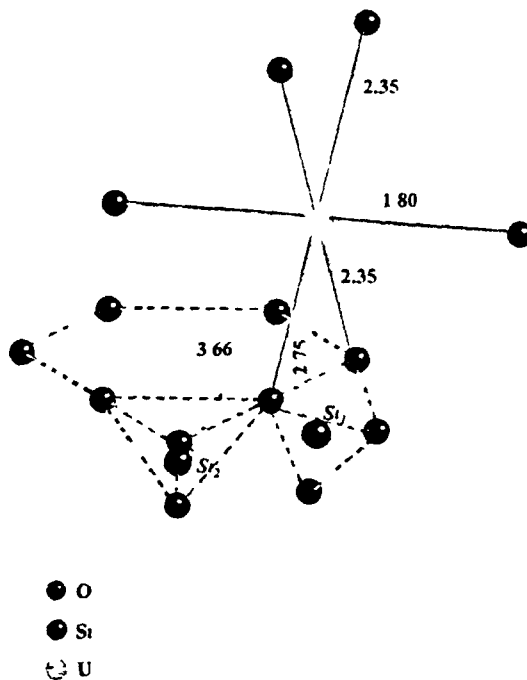


FIGURE 3 Proposed binding mechanism for uranyl species on muscovite surface (distances, in Å, are experimentally derived). Solid lines depict discrete bonds between uranium and oxygen atoms. Dashed lines indicate "through-space" distances in muscovite tetrahedral plane. Dotted lines indicate "through-space" U-Si distances. Si-O bonds in individual tetrahedra have been omitted for clarity.

short, giving a U-O-Si angle of less than 90°, which would suggest a significant amount of distortion of the surface on binding. Replacement of Si with O at this distance did not improve the fit significantly and multiple backscattering analysis also showed no improvement in fit. The peak at 3.66 Å can be fitted with two Si atoms, although inclusion of multiple backscattering further improves the fit. The feature at 3.86 Å can be fitted with four Si atoms, although a U atom at this distance gives a slightly better fit. A uranium atom at this distance could be due to formation of a uranium-(hydr)oxide precipitate which is consistent with the uptake curve (Figure 1), although it may reflect the presence of a neighboring uranyl complex on the muscovite surface.

An idealized model for coordination of a single uranyl ion on the muscovite surface is illustrated in Figure 3. Two equatorial coordination positions are filled by two corner oxygens of an [SiO₄]⁴⁻ tetrahedron. This tetrahedron forms part of one of the hexagonal rings of silicate tetrahedra which make up the tetrahedral layer in the muscovite structure, so the Si atoms of two adjacent tetrahedra are observed at a distance of 3.66 Å. In this model the axial oxygen atoms of the uranyl unit are aligned across the hexagonal cavities at the centers of the rings of tetrahedra. In the absence of distortion, the model-derived U-Si₁ distance is 2.57 Å compared with 2.75 Å from experiment, and the U-Si₂ distance is 4.03 Å compared to 3.66 Å from experiment. The experimental and calculated distances differ by up to 0.4 Å, but the calculations assume that the geometry of the tetrahedron remains undistorted on uranium coordination to the surface, and also that the bonding and non-bonding equatorial oxygens are all at equal distances from the uranium center. The discrepancies between calculation and experiment suggest that the system is significantly distorted.

Other EXAFS studies of uranium sorption on phyllosilicates have been interpreted in terms of surface complex

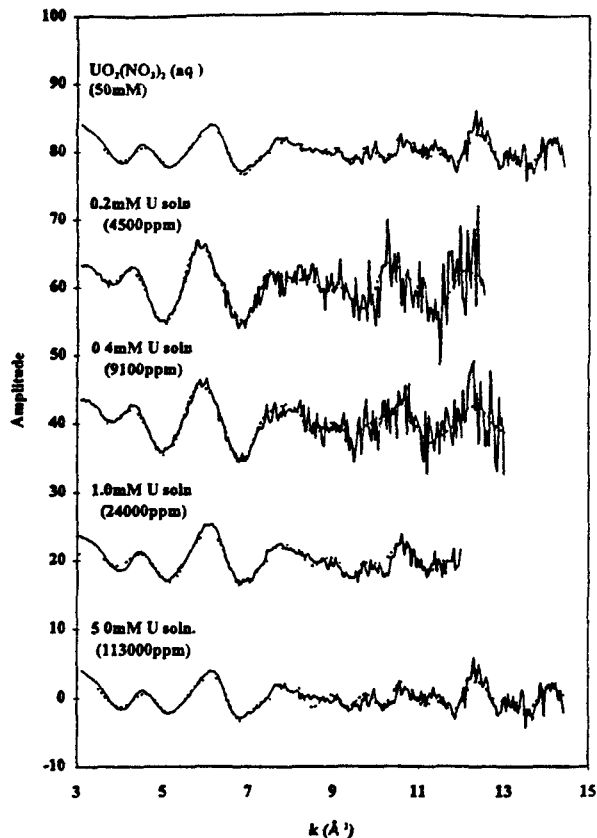


FIGURE 4 EXAFS spectra for U on mackinawite and for UO_2^{2+} in aqueous solution. For mackinawite samples original solution concentrations (mM) are given, with mass of U sorbed (μg) per g of sorbent in parentheses. Solid lines represent experimental data and dashed lines the best fit.

formation Chisholm-Brause et al (6) suggested that there are three distinct environments for oxygen atoms in the equatorial plane of the uranyl species sorbed on to the surface of montmorillonite. As surface coverage increases, there is an increase in both the number of equatorial oxygen atoms and the U-O distance. This implies that energetically more favorable surface sites are filled first. Thereafter, less favorable sites are filled as coverage increases, resulting in longer U-O distances but higher equatorial coordination numbers. Similarly, Dent et al (30) have also shown that the EXAFS spectra of uranyl species sorbed onto montmorillonite at pH 5, closely resemble those of hydrolyzed species in solution, in other words, the uranyl structure is largely retained on sorption. Unlike muscovite, the interlayer of montmorillonite can expand to $\sim 8 \text{ \AA}$, allowing a hydrated uranyl complex to enter between the layers and presenting additional sites for uranium uptake.

In the present study, the best fit is obtained with 4 ± 1 oxygen atoms in the equatorial plane. However, the comparatively high Debye-Waller factor for this shell may reflect some disorder, such as would arise given a mixture of four- and five-coordinate species. First and second shell distances in the present study agree well with those found by other workers (6, 30), however, third and fourth shell data for U-Si distances are not available for comparison.

U on Mackinawite The variation in uranium uptake on mackinawite with initial concentration in solution (Figure 1) suggests formation of a new phase on the surface (32). The EXAFS spectra (Figure 4) and their Fourier transforms (Figure 5) for four samples of increasing uranium concentration are displayed along with those for the uranyl ion in aqueous solution. It is clear that there are substantial differences

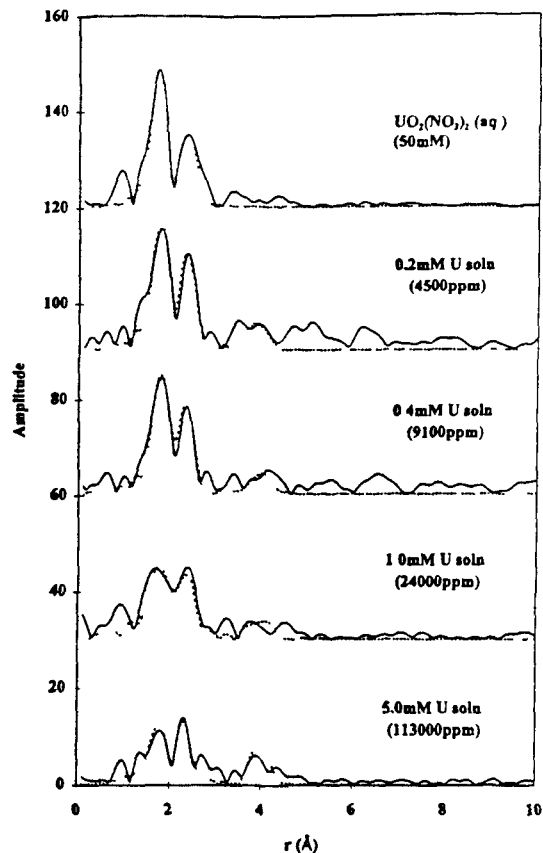


FIGURE 5 Fourier transforms for U on mackinawite and for UO_2^{2+} in aqueous solution. For mackinawite samples original solution concentrations (mM) are given, with mass of U sorbed (μg) per g of sorbent in parentheses. Solid lines represent experimental data and dashed lines the best fit.

TABLE 2 Parameters Obtained from EXAFS Data Fitting of U L(III)-Edge Spectra for Mackinawite^a

initial U soln concn (concn on mineral)	shell no	atom type	N	r (Å)	2 σ^2 (Å ²)	R
0.2 mM (4500 ppm)	1	O	2	1.81	0.005	53.7
	2	O	4	2.40	0.009	
	3	Fe	2	3.83	0.013	
0.4 mM (9100 ppm)	1	O	2	1.82	0.006	57.0
	2	O	4	2.38	0.011	
	3	Fe	2	3.96	0.016	
1.0 mM (24 000 ppm)	1	O	2	1.81	0.012	46.0
	2	O	2	2.14	0.022	
	3	O	4	2.36	0.012	
	4	Fe	2	3.97	0.015	
5.0 mM (113 000 ppm)	1	O	2	1.83	0.014	53.4
	2	O	1	2.07	0.003	
	3	O	5	2.31	0.020	
	4	Fe	2	3.97	0.008	

^a N is the coordination number (± 1), r is the interatomic distance ($\pm 0.02 \text{ \AA}$), $2\sigma^2$ is the Debye-Waller factor (\AA^2) and R is the overall goodness of fit.

between the Fourier transforms for different concentrations. The parameters (Table 2) indicate that at the two lower concentrations, the best fit is given by two axial oxygen and four equatorial oxygen atoms, with an additional Fe shell as in the inner-sphere surface complexes proposed for the hydrous iron oxide system. At higher concentrations, the best fits are obtained by splitting the second shell into two separate subshells containing oxygen atoms at 2.07–2.14 and 2.31–2.36 Å. The $\sim 2.1 \text{ \AA}$ distances are too short for

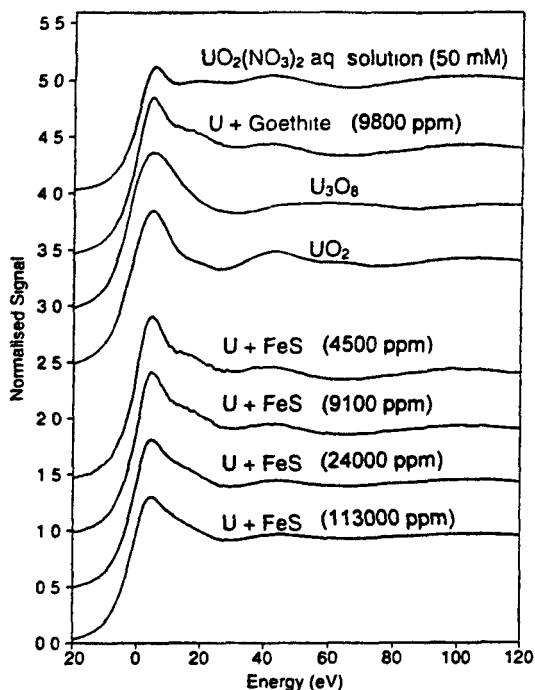


FIGURE 6 Uranium L(III)-edge XANES spectra Mass of U sorbed (μg) per g of sorbent in parentheses

equatorially bound oxygens, so binding cannot be explained solely in terms of a simple uranyl complex at higher concentrations. In addition, the Fourier transforms (Figure 5) show that the intensities of the first and second shell peaks vary greatly over the concentration range. The amplitude of a peak in the Fourier transform is a function of N and the Debye-Waller factor, so decreasing the coordination number and/or increasing the Debye-Waller factor will result in a lower amplitude. In addition, significant increases in the Debye-Waller factor of first shell data are observed with increased loading, which will also affect amplitude. However, larger Debye-Waller factors do suggest disorder which is consistent with the presence of mixed uranium species. This suggests partial reduction of uranium, leading to an increased average coordination number and a range of U-O distances between 2.07 and 2.36 Å, as found in the data fitting at higher concentrations (Table 2). Fitting the spectra with only one oxygen atom in the first shell gave higher R -factors, suggesting that there is a significant uranyl contribution even at higher surface concentrations.

The binding mechanisms in this system are obviously more complex than those of uranium on the iron hydroxide and silicate surfaces. At low surface concentrations, sorption apparently occurs in a similar way to that described for the iron hydroxide surfaces. Although mackinawite is a sulfide mineral, oxidized regions of the surface may be present, and the uranyl ion may form surface complexes in these areas (34). Once these sites are saturated, uptake may continue by coupled reduction of uranium and surface oxidation. As solution concentrations increase, a greater proportion of the uranium would be reduced, so the average number of axial oxygens would decrease and U-O distances around 2 Å, characteristic of oxide phases containing at least some U(IV) centers, e.g. U_3O_8 (35) would be observed. We may then expect a uranium atom to provide the best fit in the fourth shell at higher concentrations (Table 2), although iron gives a slightly lower R factor in both cases. Thus, at high U loadings the precipitation of a discrete uranium oxide phase containing both U(VI) and U(IV) centers, e.g. U_3O_8 or U_4O_9 may occur. This is consistent with the findings of Wersin et al. (9) who reported uptake of uranyl on pyrite and galena surfaces

associated with precipitation of a uranium oxide of mixed oxidation state.

The suggestion of phase formation is supported by the XANES data. Figure 6 shows the U L(III)-edge XANES spectra of the mackinawite samples along with spectra for U_3O_8 , UO_2 , uranyl on goethite, and aqueous uranyl nitrate. At low uranium loadings, the mackinawite XANES strongly resembles that of U on goethite, but as the U concentrations on the mackinawite surface increase, the XANES changes. The peak at 3–5 eV becomes less pronounced, while the region from 8 to 20 eV becomes more smoothly curved. At the highest surface concentration, the XANES most closely resembles that of U_3O_8 , consistent with the EXAFS data.

Acknowledgments

The support of the Natural Environment Research Council (Grant GR3/9690) and of BNFL plc is acknowledged. Thanks are due to CLRC Daresbury Laboratory for the provision of beamtime and support in carrying out the experiments.

Literature Cited

- (1) Ho C H, Doern D C *Can J Chem* 1985, 63 1100
- (2) Hsi C-K, D, Langmuir D *Geochim Cosmochim Acta* 1985 49 1931
- (3) Borovec Z. *Chem Geol* 1981 32 45
- (4) Payne T E, Waite, T D *Radiochim Acta* 1991, 52/53 487
- (5) Morse, J W, Arakaki T *Geochim Cosmochim Acta* 1993 57 3635
- (6) Chisholm Brause, C J, Conradson, S D, Buscher, C T, Eller P G, Morris, D E *Geochim Cosmochim Acta* 1994 58 3625
- (7) Morris, D E, Chisholm-Brause, C J, Barr, M E, Conradson S D, Eller, P G *Geochim Cosmochim Acta* 1994 58 3613
- (8) Waite T D, Davis, J A, Payne, T E, Waychunas G A, Xu N *Geochim Cosmochim Acta* 1994, 58, 5465
- (9) Wersin P, Hochella, M F, Jr, Persson P, Redden G, Leckie J O, Harris D W *Geochim Cosmochim Acta* 1994 58 2829
- (10) Duff M C, Amrhein, C *Soil Sci Soc Am J* 1996 60 1393
- (11) Turner, G D, Zachara J M, McKinley J P, Smith, S C *Geochim Cosmochim Acta* 1996 60 3399
- (12) Carroll, S A, Bruno, J *Radiochim Acta* 1991, 52/53, 187
- (13) Kormuier W A, Morse, J W *Geochim Cosmochim Acta* 1991 55 2159
- (14) Watson J H P, Ellwood D C *Miner Eng* 1994 7 1017
- (15) Bancroft G M, Hyland M M *Rev Mineral* 1990, 23 511
- (16) Charlet L., Manceau A. *J Colloid Interface Sci* 1992 148 443
- (17) Schwerdtmann U, Cornell R. M. *Iron Oxides in the Laboratory - Preparation and Characterisation* VCH New York 1991 Chapters 5–6 pp 61–84
- (18) Lennie A. R., Redfern S. A., Schofield P. F., Vaughan D. J. *Miner Mag* 1995 59 677
- (19) Lennie, A. R., Vaughan, D. J. In *Mineral Spectroscopy A Tribute to Roger G Burns*; Dyar, M. D., McCammon C., Schaefer M. W., Eds., The Geochemical Society Special Publication No 5 1996 p 117
- (20) Calas G, Bassett, W A., Petiau J, Steinberg D, Tchoubar D, Zarka A. *Phys Chem Miner* 1984 11 17
- (21) Brown, G E Jr, Calas G, Waychunas G A, Petiau J *Rev Mineral* 1988 18 431
- (22) Binsted N. *CLRC Daresbury Laboratory EXCURV97 program* CLRC Daresbury Laboratory Warrington 1997
- (23) Lee P A, Pendry J B *Phys Rev B* 1975 11 2795
- (24) Gurman, S J, Binsted N, Ross I *J Phys C Solid State Physics* 1984 17, 143
- (25) Gurman S J, Binsted N, Ross I *J Phys C Solid State Physics* 1986 19 1845
- (26) Hedin L, Lundqvist S *Solid State Phys* 1969 23 1
- (27) Binsted N, Strange R W, Hasnain S S *Biochemistry* 1992 31, 12117
- (28) Rehr J J, Albers R C *Phys Rev B Condensed Matter* 1990 41 8139
- (29) Langmuir D *Geochim Cosmochim Acta* 1978 42 547
- (30) Dent A J, Ramsay J D F, Swanton S W *J Colloid Interface Sci* 1992 150 45

- (31) Tsunashima A, Brindley G W, Bastovanov M *Clays Clay Miner* 1981 29 10
(32) Parkman, R H, Charnock J M, Bryan N D, Livens F R, Vaughan D J *Am Miner* 1999 84 407
(33) Bargar, J R, Reitmeyer R L, Davis J A *Environ Sci Technol* 1999 33 (14) 2481
(34) McIntyre, N S, Zetaruk D G *Anal Chem* 1977 49 521

(35) Wells A F *Structural Inorganic Chemistry* 4th ed Clarendon Oxford 1975

Received for review June 28, 1999 Revised manuscript received December 20 1999 Accepted December 20 1999

ES990703K



Nature, 397 (1999) 66-69

letters to nature

Re and Al₂O₃ were heated with laser beams from both sides. Acting like planar heat sources, the two hot plates eliminate the axial temperature gradient in the sample between the plates. Temperature variation is less than 3% within roughly 30 μm diameter at 2500 K. Before the melting experiments the sample was scanned with a laser beam and heated to about 2000 K to reduce the pressure gradient and to produce a high-pressure solid-phase assemblage. For stable and smooth temperature control, temperatures were increased by adjusting an aperture placed near the beam exit, stepwise, instead of by adjusting power. Each step corresponds to a 50–100 K increase. A 30-μm spot was homogeneously heated by opening the aperture (increasing the step). At the onset of melting temperature remains constant or drops slightly with the step increment and then drastically increases (>400 K) within one step. To ensure the reliability of the melting criteria used in this study, we conducted melting experiments at pressures (16–27 GPa) overlapped by the multi-anvil apparatus and the diamond anvil cell using the same starting material and obtained consistent melting temperatures (Fig. 4). We also used the same melting criteria to determine the melting temperature of MgSiO₃-perovskite previously studied by other investigators, and our results agree with these recent determinations^{13,14} (Fig. 3). The temperature runaway phenomena near the onset of melting observed in simple and complex samples were probably a result of the latent heat of melting followed by melt migrating away from the heated spot because of the large thermal pressure and, finally, the Re foils would have been heated without sample in between. No chemical reaction between Re and sample was observed in the multi-anvil experiments on a scale of 1 μm. The melting temperatures reported here are the last temperatures before melting sets in. Pressures were measured using a ruby fluorescence technique after each measurement of melting temperature.

Received 22 June; accepted 12 October 1998

1. Irifune T & Ringwood A E. Phase transformations in subducted oceanic crust and buoyancy relationships at depths of 600–800 km in the mantle. *Earth Planet Sci Lett* 117, 101–110 (1993).
2. Ringwood A E. Role of the transition zone and 660 km discontinuity in mantle dynamics. *Phys Earth Planet Inter* 26, 3–24 (1994).
3. Morita, C. M. & Fei Y. Mineralogy of Martian interior up to core-mantle boundary pressures. *J Geophys Res* 103, 5231–5244 (1997).
4. Irifune T, Ringwood A F & Hibberd W O. Subduction of continental crust and terrigenous and pelagic sediments: an experimental study. *Earth Planet Sci Lett* 126, 351–368 (1994).
5. Irifune T, Kazumi T & Ando J. An experimental study of the garnet perovskite transformation in the system MgSiO₃-MgAl₂SiO₅-O₂. *Phys Earth Planet Inter* 96, 147–157 (1996).
6. Hirose, K. & Fei Y. Majorite perovskite transformation on the iron Mg₉₀O MgAl₁₀O₂ and its role in the dynamics at the 660-km discontinuity. *Phys Earth Planet Inter* (submitted).
7. Keown, S. L., Fitz Gerald, J. D. & Shelley J M. Mineralogy and dynamics of a pyroxite lower mantle. *Nature* 393, 252–255 (1998).
8. Faust I & Kretz R. The stability and equation of state of stauropite garnet synthesized from natural basalt at mantle conditions. *Geophys Res Lett* 23, 3377–3380 (1996).
9. Keown S E, Fitz Gerald, J. D. & Shelley J M. G. Mineral chemistry and density of subducted basaltic crust at lower-mantle pressures. *Nature* 372, 767–769 (1994).
10. Irifune T & Ringwood A E. Phase transformation in a harzburgite composition to 26 kPa: implications for dynamical behaviour of the subducting slab. *Earth Planet Sci Lett* 86, 365–376 (1987).
11. Shen G, Mao H & Hemley R S. Laser-heated diamond anvil cell technique: double sided heating with multimode Nd:YAG laser. *Proc SPIE* 391, 148–152 (1994).
12. Yasuda A, Fujii T & Kizuka K. Melting phase relations of an anhydrous mid-ocean ridge basalt from 1 to 20 GPa: implications for the behavior of subducted oceanic crust in the mantle. *J Geophys Res* 99, 9401–9414 (1994).
13. Zerr A & Boehler R. Melting of (Mg,Fe)SiO₃-perovskite to 625 kilobars: indication of a high melting temperature in the lower mantle. *Science* 262, 552–558 (1993).
14. Shen G & Lazor P. Measurement of melting temperatures of some minerals under lower mantle pressures. *J Geophys Res* 100, 17499–17513 (1995).
15. Zerr A, Berghaus G & Boehler R. Melting of CaSiO₃ perovskite to 450 kbar and Fe in situ measurements of lower mantle geotherms. *Geophys Res Lett* 24, 909–913 (1997).
16. Frennoll D C & Campbell, T. Melting of enstatite (MgSiO₃) from 10 to 16.5 GPa and the forsterite (Mg₂SiO₄) mantle (MgSiO₃) eutectic at 16.5 GPa: implications for the origin of the mantle. *J Geophys Res* 98, 15771–15777 (1993).
17. Zerr A, Dreyer A & Boehler R. Subduct of Earth's deep mantle. *Nature* 381, 243–246 (1999).
18. Kendall J M & Silver P. Constraints from seismic anisotropy in the lowermost mantle. *Nature* 381, 419–421 (1998).
19. Kendall J M & Silver P. Investigating causes of D anisotropy by ACU Modeling. (in the press).
20. Williams, Q & Garnero F. Seismic evidence for partial melt at the base of Earth's mantle. *Science* 273, 1526–1530 (1996).
21. Revenaugh, T. & Meyer R. Seismic evidence of partial melt within a possibly stagnant, low-velocity layer at the base of the mantle. *Science* 277, 670–673 (1997).
22. Simon F F & Glazov G. Fusion pressure curve. *Z. Anorg Allg Chem* 178, 300 (1929).
23. Kraut G A & Kennedy G C. New melting law at high pressures. *Phys Rev Lett* 10, 504–507 (1966).
24. Boehler R. Melting temperature of the Earth's mantle and core. *Earth Thermal Structure Annu. Rev. Earth Planet Sci.* 15–40 (1994).
25. Mao H, Chen L C, Hemley R S, Yehouan A P & Wu Y. Stability and equation of state of CaSiO₃ perovskite to 14 GPa. *J Geophys Res* 96, 17843–17844 (1991).

Acknowledgements: We thank W. Minarik, J. A. Scott, G. Shew and S. Shieh for discussions. This research was supported by the NSF, the Carnegie Institution of Washington, and Japan Science and Technology Agency.

Correspondence and requests for material should be addressed to T.F. (e-mail: tef@ucl.ac.uk).

Migration of plutonium in ground water at the Nevada Test Site

A. B. Kersting*, D. W. Efrud†, D. L. Finnegan†, D. J. Rokop†, D. K. Smith* & J. L. Thompson†

* Isotope Sciences Division, PO Box 808 [L-231] Lawrence Livermore National Laboratory Livermore, California 94550 USA

† Chemical Science and Technology Division MS 1514, Los Alamos National Laboratory, Los Alamos New Mexico 87545 USA

Mobile colloids—suspended particles in the submicrometre size range—are known to occur naturally in ground water^{1,2} and have the potential to enhance transport of non-soluble contaminants through sorption. The possible implications of this transport mechanism are of particular concern in the context of radionuclide transport. Significant quantities of the element plutonium have been introduced into the environment as a result of nuclear weapons testing and production, and nuclear power-plant accidents. Moreover, many countries anticipate storing nuclear waste underground. It has been argued that plutonium introduced into the subsurface environment is relatively immobile owing to its low solubility in ground water³ and strong sorption onto rocks⁴. Nonetheless, colloid-facilitated transport of radionuclides has been implicated in field observations^{5,7}, but unequivocal evidence of subsurface transport is lacking^{2,8,9}. Moreover, colloid filtration models predict transport over a limited distance resulting in a discrepancy between observed and modelled behaviour⁷. Here we report that the radionuclides observed in groundwater samples from aquifers at the Nevada Test Site where hundreds of underground nuclear tests were conducted, are associated with the colloidal fraction of the ground water. The ²⁴⁰Pu/²³⁹Pu isotopic ratio of the samples establishes that an underground nuclear test 3 km north of the sample site is the origin of the plutonium. We argue that colloidal groundwater migration must have played an important role in transporting the plutonium. Models that either predict limited transport or do not allow for colloid facilitated transport may thus significantly underestimate the extent of radionuclide migration.

The Nevada Test Site (NTS) was the location of 828 underground nuclear tests conducted by the United States between 1956 and 1992¹⁰ (Fig. 1a). As a result, the NTS contains a large inventory (>10⁶ Ci) of radioactive material deposited in the subsurface and thus provides a unique opportunity for studying the transport of radionuclide contaminants. During an underground nuclear test, temperatures exceed 10⁴ K locally and ~70 tonnes of rock are vaporized and another 700 tonnes of rock are melted for every kiloton (kt) of explosive yield¹¹. Most refractory radionuclide species (for example actinides (except U), rare earths and alkaline earths) are incorporated into the melt glass that coalesces at the bottom of the cavity. The volatile species (for example, alkali metals, U, Sb, I, Ru and gases—Ar, Kr, Xe) are more broadly distributed in the cavity and overlying rubble chimney created directly above the cavity¹².

Samples were collected in the northwestern section of the NTS (Fig. 1a) where thick sequences of ash-flow tuffs and rhyolitic lava flows dominate the geology^{13,14}. Hydrological gradients in the study area suggest a southwestward and southward flow of ground water with estimated flow velocities ranging from 1 to 80 m yr⁻¹ (ref. 15). The ER-20-5 well cluster is located 280 m southwest of the Tybo test site and 1.5 km south of the Benham test site (Fig. 1b). The ER-20-5 wells no. 1 and no. 3 were screened at a depth of 701–784 m and 1046–1183 m respectively.

Groundwater samples were pumped into 200 l drums on three separate occasions over a 16-month period. Unfiltered groundwater

8

IPC = 0057E

amples were analysed for tritium (^3H), γ -ray-emitting radionuclides and Pu isotopes. Additional 200-l groundwater samples from well no 1 were collected on the second and third sampling campaigns and filtered in series using 1,000-nm, 50-nm and ~ 7 -nm (100,000 nominal molecular mass) filter sizes. The particulate material ($>1,000$ nm), two colloidal fractions (1,000–50 nm and 50–7 nm) and the ultrafiltrate or dissolved fraction ($< \sim 7$ nm) were separately analysed for ^3H , γ -ray-emitting radionuclides and Pu isotopes¹⁵.

Surface soil samples were collected in the vicinity of the Benham and Tybo nuclear test sites and their $^{240}\text{Pu}/^{239}\text{Pu}$ isotope ratios measured. Archived melt glass material collected from the cavity region immediately after the detonation of the Benham and Tybo tests was re-analysed for its $^{240}\text{Pu}/^{239}\text{Pu}$ isotope composition and compared to data previously obtained during the US nuclear test programme. Aliquots from the melt glass were analysed at Los Alamos National Laboratory as well as Lawrence Livermore National

Laboratory to provide external laboratory comparison. Additional experimental details from this study are given elsewhere^{16,17}.

Tritium and low specific activities of cobalt (Co), caesium (Cs), europium (Eu) and Pu isotopes were detected in the unfiltered ground water (Fig 2). The levels of radioactivity measured from ground water collected from well no 3 are significantly lower (1,000–20 times lower) than those measured in ground water from well no 1. Eu isotopes were not detected in ground water from well no 3 but may be present below the level of detection ($\sim 10^{-3}$ Bq l⁻¹). Figure 2c illustrates that the same radionuclides and similar levels of radioactivity were detected in the ground water samples obtained from well no 1 during the three different sampling periods. Analogous results were obtained for ground water samples from well no 3 (data not shown).

Filtering removed most of the radionuclides from solution, but had essentially no effect on the ^3H concentration in the filtrates. We found that $>99\%$ of the Eu and Pu isotopes $\sim 91\%$ of the Co, and

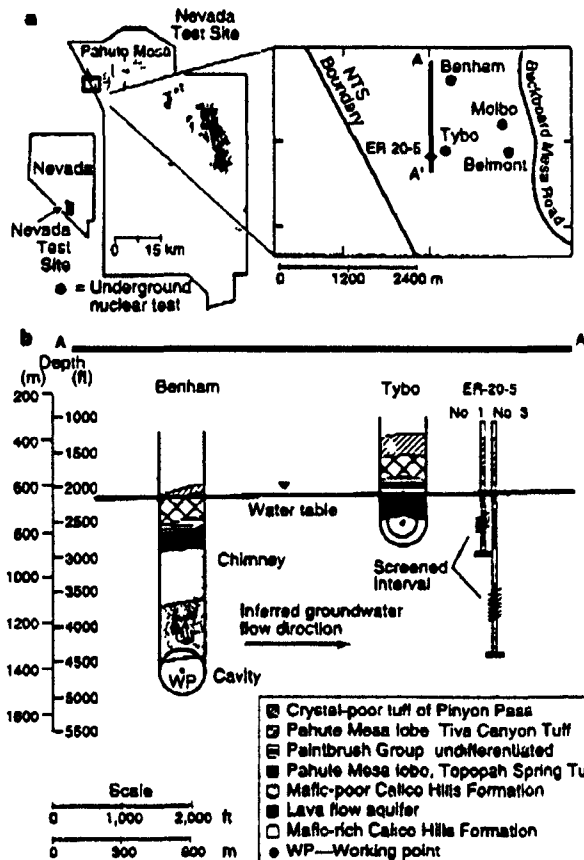


Figure 1 Location and geology of the study area. **a** Map of the Nevada Test Site showing the locations of all detonated underground nuclear tests. An enlarged map of the field area in Pahute Mesa is also shown, giving the location of the well cluster ER 20-6 and all other nearby underground nuclear tests. Molbo (1982) and Belmont (1988) have an announced yield between 20 and 150 kt. **A-A** is a north-south cross-section projecting the Benham and Tybo nuclear tests relative to the ER 20-6 well cluster. Well no 3 is located ~ 30 m south of well no 1. The Tybo test was detonated in moderately welded tuff on 14 May 1975 at a depth of 765 m and had an announced yield between 200 and 1000 kt. Benham was detonated in zoned bedded tuff on 19 December 1966 at a depth of 1402 m with a nuclear yield of 1180 kt. The working point (WP) denotes the location of the nuclear device before detonation. The radius of the cavity is a function of the nuclear yield, density of the rock type and depth of burial (distance from ground surface to WP). Benham has a calculated cavity radius of 98 m and Tybo between 62 and 105 m based on the unclassified range in yield.

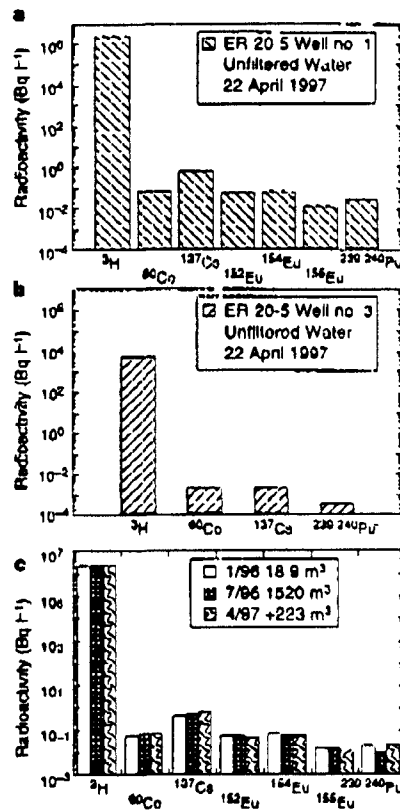


Figure 2 Comparison of radioactivity detected in unfiltered groundwater samples from ER 20-6 well cluster. Groundwater chemistry of ER 20-6 no 1 in mg l⁻¹ is as follows: [Cl] = 33, [SO₄] = 36.0, [Na⁺] = 70.0, [K] = 31, [Ca²⁺] = 3.2, [Mg²⁺] = 0.1, pH 8.4. For the purposes of comparison, all data were decay corrected to 22 April 1997, the time of the third sampling. **a** Concentration of radioactivity measured in unfiltered ground water from the shallower aquifer pumped from well no 1. **b** Concentration of radioactivity measured in unfiltered ground water from the deeper aquifer pumped from well no 3. **c** Comparison of the radioactivity detected in the three groundwater samples collected from well no 1 over the duration of the field experiment. The first sample was collected after 18.9 m³ (5,000 gallons) were pumped, the second after 1.62 $\times 10^3$ m³ (401,000 gallons). The pumps were shut down and restarted the next spring. An additional 2.23 $\times 10^3$ m³ (58,000 gallons) of ground water was pumped before the third sample was collected. A total of 1.76 $\times 10^3$ m³ were pumped from well no 1 and 2.19 $\times 10^3$ m³ from well no 3. Pumping rate is 0.030 m³ min⁻¹.

9

letters to nature

95% of the Cs in the ground water from well no 1 were associated with the colloidal and particulate fractions (Fig 3a)

To determine the source of the radionuclides, and hence the distance they have been transported, we use the ²⁴⁰Pu/²³⁹Pu isotope ratio to 'fingerprint' the source of the observed Pu in the ground water Figure 3b shows the normalized ²⁴⁰Pu/²³⁹Pu isotope ratios measured in this study The ²⁴⁰Pu/²³⁹Pu isotope ratio of the unfiltered ground water from well no 1 matches those of the unfiltered ground water from well no 3 and the colloidal and particulate fraction from well no 1 In addition, it uniquely matches the Benham nuclear test and no other (Each nuclear detonation in the study area is characterized by a unique ²⁴⁰Pu/²³⁹Pu isotope ratio.) The ²⁴⁰Pu/²³⁹Pu isotope ratio of the ground water is distinctly different from that of the surface soil samples, eliminating surface contamination as a possible source for the Pu detected in the ground water

The particulates and two different colloidal size fractions were analysed by X-ray diffraction (XRD) and scanning electron micro-

scopy (SEM) The material was composed of clays (illite and smectite), zeolites (mordenite and clinoptilolite/heulandite) and cristobalite The same mineral assemblage was detected in all three size fractions (>1 μm, 1,000-50 nm, and 50-~7 nm) Figure 4 shows SEM images of two distinct morphologies observed, the flat platy minerals and the rod shaped minerals are likely to be clays (illite) and zeolite (mordenite), respectively

Clays and zeolites are common secondary minerals in altered rhyolitic tuff and smectite, clinoptilolite and mordenite have been specifically identified in the rocks on Pahute mesa¹² and elsewhere in volcanic tuffs at the NTS¹⁰ Smectite has also been identified as an alteration mineral formed during dissolution of nuclear waste glass¹⁹ The colloidal minerals identified in ER-20-5 ground water from well no 1 are consistent with the secondary minerals observed in ground water collected from volcanic tuff aquifers located in the southwestern part of the NTS^{20,21}

Strontium, Cs, Co and actinides (including Pu) have been shown to strongly sorb to clays and zeolites as a result of their large cation-exchange capacity^{22,23} For example, Pu sorption experiments involving clinoptilolite with grain sizes between 75 and 500 μm and NTS water with a pH of 7 yielded distribution coefficients of $K_d > 500 \text{ ml g}^{-1}$ (ref 5) The zeolite particles and colloids observed in the present study fall within the micrometre and submicrometre size range Their reduced size will be associated with larger surface areas and is therefore likely to result in higher K_d values In fact, recent experiments on the sorption of Pu to montmorillonite suggest that this process may be irreversible on the timescale of the laboratory experiments²⁴ (~1 year)

The data obtained in this study suggest that Pu and other radionuclides are transported as colloidal material Although Pu has been shown experimentally to strongly sorb to clays and zeolites, Pu can also exist as an intrinsic colloid, composed of Pu oxide²⁵ Both types of colloids have the capacity to be transported by ground water From this study, we cannot distinguish the colloidal form of the Pu and further study is needed We suggest that Co, Cs and Eu are sorbed onto the colloidal sized clays and zeolites in the ground water as they do not form intrinsic colloids

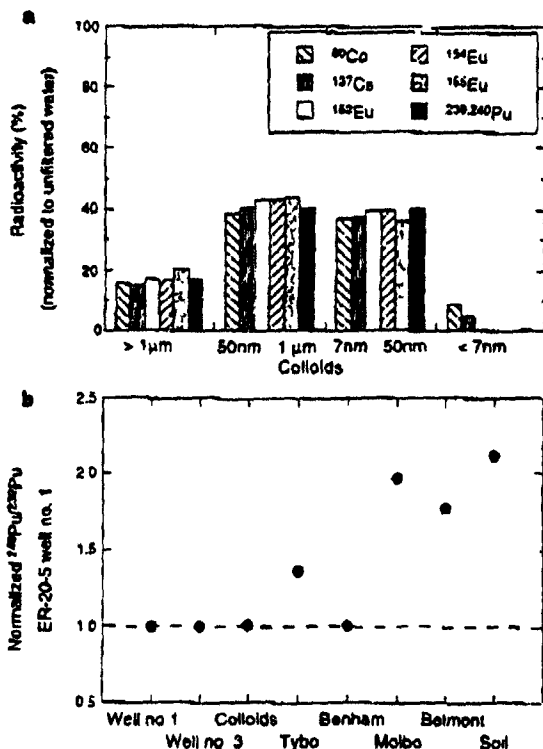


Figure 3 Radioactivity of the colloidal minerals and comparison of Pu isotope ratios from ER 20-5 ground waters to other nuclear tests a Comparison of the radioactivity of the colloids collected on the different filter sizes and the ultrafiltrate fraction Data are normalized to the total radioactivity measured in the unfiltered water The ultrafiltrate is the water that passed through all the filters (<~7 nm) Filtration occurred in series A tangential filtration system was used for the 100 000 nominal molecular mass (~7 nm) size filters b Comparison of the ²⁴⁰Pu/²³⁹Pu isotope ratios of different samples in this study normalized to the radioactivity measured in ER 20-5 no 1 Precision is ± 15% The errors plotted are smaller than the symbols used Results of the Pu isotopic analyses of the archived melt glass material collected from the cavity region immediately after the detonation of Benham and Tybo from both laboratories agree to within 15% and also match the original values measured immediately following the nuclear tests Total laboratory procedural blanks had ~2 pg Pu significantly below the concentrations analysed and did not contribute to the isotope ratio measured The concentrations of Pu detected in the soil samples were extremely low (~4 pg Pu per g sample) and the isotopic ratios distinctly different from the ground water Values plotted are averages ER 20-5 no 1 N = 3 ER 20-5 no 3 N = 2 Colloids N = 4 Tybo N = 6 Benham N = 12 Molbo N = 7 Belmont N = 4 and Soil N = 2 Here N is the number of samples averaged

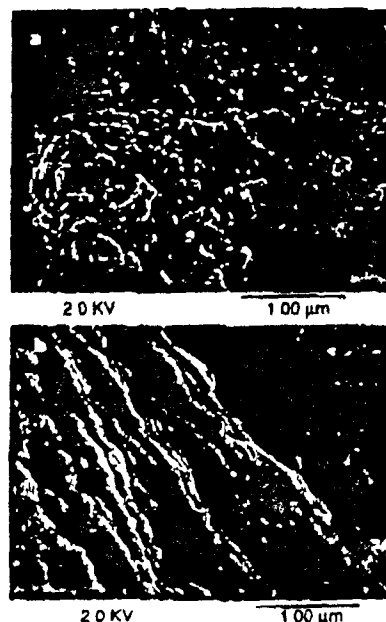


Figure 4 High resolution SEM images of the colloids in ER 20-5 no 1 a The tabular flat shaped morphology of the zeolite mordenite b the platy appearance of the clay illite The two distinct morphologies were observed in all three size fractions (> 1 μm, 1000-50 nm, and 50-~7 nm)

The maximum measured concentration of Pu at the ER-20-5 site is $\sim 10^{-14}$ M. This value is lower than the solubility limits of $\sim 10^{-14}$ M that have been experimentally determined for the Pu(V) species likely to be present in NTS ground water⁴. The calculated solubility limits (10^{-12} – 10^{-17} M), obtained by assuming that Pu(IV) is in thermodynamic equilibrium^{26,27}, bracket the maximum measured Pu concentration. It thus seems that the Pu concentrations in the ground water at ER-20-5 were too low to lead to the precipitation of a solid Pu phase. Our results indicate that <1% of the observed Pu is in the dissolved fraction of the ground water. This finding and the previously reported results of Pu sorption experiments⁴ are most consistent with Pu migrating as colloidal material and not as a dissolved phase. The concentration of Pu measured is small, and represents only a small fraction of the total Pu associated with the Benham nuclear test.

Based on 40 years of re-drilling underground nuclear test cavities and collecting melt glass samples for test diagnostics, it has been observed that the majority (~98%) of the refractory radionuclides (such as Pu) are incorporated into the melt glass that forms at the bottom of the test cavity^{22,28}. In field studies where ground water can be eliminated as a possible transport mechanism, radionuclides were detected at a maximum of a few hundred metres from the original detonation point, and were attributed to gas movement through fractures, or fracture injection of vaporized material at detonation time^{29,30}. The possibility that Pu from the Benham test site was blasted and deposited >13 km away, in two distinct aquifers separated by 300 m vertically and 30 m horizontally, seems highly unlikely. However, some fraction of the Pu may have been initially injected through fractures a few hundred metres and subsequently transported by ground water.

Molbo, Belmont and Tybo nuclear tests were all detonated after Benham. Although shock waves resulting from underground nuclear blasts can induce radial fractures out to a maximum distance of a few hundred metres (ref. 30), it is unlikely that these detonations blasted material from Benham to ER-20-5, as they were all smaller detonations and by inference shallower. In addition, Pu from these subsequent three tests was not detected in the ground water at ER-20-5.

The high pumping rates ($0.03 \text{ m}^3 \text{ min}^{-1}$) employed may create shear stresses sufficient to generate an increase in the concentration of colloids and thus prevent a quantification of the ambient colloidal load and, by inference, a determination of the minimum or maximum concentration of Pu in the ground water. But the isotope ratio of the Pu measured in ground water from ER-20-5 nevertheless clearly establishes that the radionuclide originates from a specific nuclear event, ~13 km to the north. The present work thus demonstrates that Pu is not immobile in the subsurface, but can be transported over significant distances. Pu transport models that only take into account sorption and solubility may therefore underestimate the extent to which this species is able to migrate in ground water. □

Received 24 February; accepted 6 October 1998

1. Dequckter, C. et al. Colloids in water from a subsurface fracture in granitic rock, Grand test site, Yucca Mountain, Nevada. *Chemical Geology* **33**, 603–610 (1999).
2. McDowell, Boyer, L. M. Chemical mobilization of micron sized particles in saturated porous media under steady flow conditions. *Environ. Sci. Technol.* **26**, 586–593 (1992).
3. Ryan, J. N. & Elimelech, M. Colloid mobilization and transport in groundwater. *Colloids Surfaces A Physicochem. Eng. Aspects* **107**, 1–56 (1996).
4. Nitsche, M. et al. Measured Solubilities and Speciations of Neptunium, Plutonium, and Americium in a Typical Groundwater (11) from the Yucca Mountain Region. *Milestone Report 3010-WBS 1.2.3.4.1.3.1* (Rep. LA 12562-MS, Los Alamos National Laboratory 1993).
5. Tracy, J. P. et al. Radionuclide Sorption in Yucca Mountain Tuffs with 11 Wall Water Neptunium, Uranium, and Plutonium (Rep. LA 12956-M5, Los Alamos National Laboratory 1996).
6. Buddemeier, R. W. & Hsu, J. R. Transport of colloidal contaminants in groundwater radionuclide migration in the Nevada Test Site. *Appl. Geochem.* **3**, 535–548 (1988).
7. McCrease, W. R., Polyzos, W. L., Basington, E. M., Nelson, D. M. & Orlandini, E. A. Mobility of plutonium and americium through a shallow aquifer in a semiarid region. *Environ. Sci. Technol.* **24**, 218–224 (1990).
8. McCarthy, J. P. & Dequckter, C. in *Environmental Radionuclides* (eds Butler, J. & van Leeuwen, H. P.) 247–315 (Lewin, Ann Arbor 1993).
9. Marty, R. C., Bennett, D. & Thullen, P. Mechanism of plutonium transport in a shallow aquifer in

10. *United States Nuclear Test—July 1945–September 1991* (DOE/NV 209 (Rev. 14) US Department of Energy/Nevada Field Office 1994).
11. Smith, D. K. Characterization of nuclear explosive rock debris. *Radiation Acta* **49**, 157–167 (1974).
12. Bogle, J. Y. et al. R. Levy, H. B. & Namsponi, L. D. Information Pertinent to the Migration of Radioisotopes in Ground Water at the Nevada Test Site (Rep. UCRL 52072A, Lawrence Livermore National Laboratory 1976).
13. Blinnenberg, R. K. & West, J. B. J. Geology of the eastern part of Pahute Mesa, Nevada Test Site, Nye County, Nevada. *Geol. Surv. Prof. Pap.* **712**, B (1973).
14. Luczak, R. J., Cole, J. L., Sawyer, D. A. & Trudeau, U. A. Summary of hydrogeologic conditions and ground water flow at the Nevada Test Site. *Nye County, NV* (Rep. 96-4109, US Geological Survey 1996).
15. Pariza, K. L., Kumbhakar, G. W., Armpo, V. M. & Elrod, D. W. Isotopic analysis of nanogram quantities of plutonium by using a 242Pu ionization source. *Int. J. Mass Spectrom. Ion Phys.* **64**, 17–24 (1985).
16. Thompson, J. L. Laboratory and Field Studies Related to radionuclide migration at the Nevada Test Site. *October 1, 1986–September 30, 1997* (Rep. LA 13419 PR Ed., Los Alamos National Laboratory 1998).
17. Smith, D. K. et al. *Hydrologic Resources Management Program and Underlying of Test Area Operations* (Final FY 1997 Progress Report) (Rep. UCRL 113-116793 Ed., Lawrence Livermore National Laboratory 1998).
18. Brostrom, D. E., Bush, D. L. & Warren, R. G. Distribution and chemistry of isogenic minerals at Yucca Mountain, Nye County, Nevada. *Clays Clay Miner.* **35**, 89–110 (1987).
19. Bates, J. K., Bradley, J. J., Toppin, A., Bradley, C. R. & Buchholz, G. R. M. Colloid formation during waste form revision: implications for nuclear waste disposal. *Science* **256**, 649–651 (1992).
20. Viani, R. E. & Martin, S. J. Groundwater Colloid Characterization (UCRL—Lawrence Livermore National Laboratory 1996).
21. Kingston, W. L. & Whitbeck, M. Characterization of Colloids Found in Various Groundwater Environments in Central and Southern Nevada. (Rep. DOE/NV/1018) 36, Desert Research Inst., Las Vegas 1991).
22. Goring, R. N. J. & Muckley, D. E. Kinetics of cesium sorption on illite. *Chemical Geology* **36**, 1137–1144 (1992).
23. Fritzsche, H. B., Rindberg, R. S. & Mitchell, A. J. Actinide sorption in granitic soil minerals as a function of pH and anion/particle/colloids. *Radiation Acta* **44/45**, 111–117 (1988).
24. Tracy, J. P., Liu, N., Cotter, C. R. & Kitten, H. D. Iron Oxide Colloid Transport. *Proc. 11th Int. Conf. on Heavy Metals in the Environment* (Am. Chem. Soc., Las Vegas 1997).
25. Silva, R. J. & Nitsche, M. Actinide environmental chemistry. *Radiation Acta* **70/1**, 371–396 (1994).
26. Stout, R. B. & Lender, H. Preliminary Waste Form Characterization Report Version 1.0 (Rep. UCRL 10 108714 Rev. 1, Lawrence Livermore National Laboratory 1994).
27. Guillaumont, R. & Adirak, I. P. Behavior of environmental plutonium at very low concentrations. *Radiation Acta* **58/59**, 51–60 (1993).
28. Le, Y. H. B. On Evaluating the Hazards of Groundwater Contamination by Radioactivity from an Underground Nuclear Explosion (Rep. UCRL 51276, Lawrence Livermore National Laboratory 1972).
29. Nitsche, G. J. & Thompson, J. L. Underground Radionuclide Migration at the Nevada Test Site (Rep. DOE/NV 36 US Department of Energy Nevada Field Office 1992).
30. Smith, D. K., Nagle, R. J. & Kumbhakar, J. M. Transport of gaseous uranium products adjacent to an underground nuclear test cavity. *Radiation Acta* **73**, 17–183 (1996).
31. Hudson, R. C., Ingham, K. M., Keller, C. E. & Smith, C. W. Cavity Radius Limitations (Rep. LA 9 11 C, Los Alamos National Laboratory, Murray 1981).

Acknowledgements: We thank B. A. Martinez, F. R. Ruess, J. W. Chamberlin and G. P. Russ for help with sample analysis, and J. R. Tracy, B. E. Viani, R. W. Loughhead, H. J. Sh. F. J. Brown, J. F. Wild and G. B. Hudson for discussions. This work was funded partly by the Underground Test Area Project sponsored by US Department of Energy Nevada Operations Office. Work was performed under the auspices of the US Department of Energy by Los Alamos National Laboratory and Lawrence Livermore National Laboratory.

Correspondence and requests for materials should be addressed to A.B.K. (e-mail: karsting@llnl.gov).

Patterns of recruitment and abundance of corals along the Great Barrier Reef

T. P. Hughes, A. H. Baird, E. A. Dinsdale, N. A. Moltschanlowsky*, M. S. Pratchett, J. E. Tanner & B. L. Willis

Department of Marine Biology, James Cook University, Townsville, Queensland 4811, Australia

Different physical and biological processes prevail at different scales^{1–4}. As a consequence, small-scale experiments or local observations provide limited insights into regional or global phenomena^{5–8}. One solution is to incorporate spatial scale explicitly into the experimental and sampling design of field studies to provide a broader, landscape view of ecology^{1–4}. Here we examine spatial patterns in corals on the Great Barrier Reef, across a spectrum of scales ranging from metres to more than 1,700 km. Our study is unusual because we explore large scale patterns of a

*Present address: Department of Aquaculture, University of Tasmania, Launceston, Tasmania 7250, Australia.

Nature, 317, 56-59 (1999)

are ingested with lizards — rather than directly from the plant — is supported by observation and by a strong correlation between lizard remains and *Lycium* seeds in the pellets. The seeds in the shrike pellets had a higher germination rate (64%) than those from lizard droppings (50%) or directly from the plant (54%) showing that their experience in passing through two vectors had increased their potential for immediate germination.

Lizards are an effective dispersal system for *Lycium* on Alegranza, but movement of the plant between islands using the lizard as a vector is likely to be rare (although not impossible³). Movement of the seeds from lizard to bird however, presents a range of opportunities for island-dwelling plants, giving them a far greater chance of moving to new islands. Because the seeds are retained in the shrike's gizzard for less than an hour, feeding and flight must follow in rapid succession if dispersal by this means is to be effective. Like so many other events in island biology given enough time it will probably happen.

The significance of predators as secondary dispersers of fruits and seeds is likely to be limited to specific situations. In Britain

the sparrowhawk (*Accipiter nisus*) is known to exploit situations where flocks of fruit-eating birds are feeding⁴ so again, the predator could easily ingest seeds with the prey. But the transfer of seeds from one bird to another in this way is unlikely to have much of an effect on seed dispersal. On Alegranza, *Lycium* seeds have also been found in kestrel (*Falco tinnunculus*) pellets, but these may have been derived from fruit-eating birds rather than lizards. Only where seed transfer involves increased mobility and range (as in the plant-lizard-bird sequence) will new dimensions of dispersal be opened. Predation can then assume a biogeographically significant role. □

Peter D. Moore is in the Division of Life Sciences, King's College, Campden Hill Road, London W8 7AH UK

e-mail: peter.moore@kcl.ac.uk

1. Nagesh, M., Delgado, I. D. & Medina, F. M. *J. Ecol.* 86, 666-671 (1998)
2. van der Pul, L. *Principles of Dispersal in Higher Plants* (Springer, Berlin, 1987)
3. Fridolfsson, S. *Wetland* (Wiley, New York, 1975)
4. Whittaker, R. L. & Brown, S. H. *J. Biogeogr.* 21, 45-58 (1994)
5. Cerdano, F. J., Hodge, K. & Dudley, J. *Nature* 392, 536 (1999)
6. Simon, H. & Simon, D. *Birds and Berries* (T. & A. D. Cooper, Luton, 1988)

Geochemistry

Colloidal culprits in contamination

Bruce D. Honeyman

Perhaps nowhere have the details of contaminant transport in groundwater systems been more contentious than in the area of nuclear waste disposal. Over the past decade, the discovery of colloidal forms of actinides, such as plutonium (Pu), has often been at the centre of concern over underground storage of radionuclides. On page 56 of this issue¹ Kersting *et al.* provide an illustration of the striking influence colloids² may have on contaminant transport. The authors have studied groundwater migration of Pu from a nuclear detonation site in Nevada. However, the particular significance of their report lies in reinforcing a general awareness of colloid-facilitated contaminant transport.

As late as the early 1980s, a groundwater contaminant was generally assumed to occupy one of two phases: a stationary phase consisting of aquifer solids, and a mobile, aqueous phase that serves as the medium for the movement of dissolved chemical species. In such a system, the rate of contaminant transport depends on the groundwater transport velocity, of course, but also on the distribution of the contaminant between the two phases. The greater the extent to which a contaminant partitions into the immobile phase, the slower its average transport velocity in the groundwater (Fig. 1)

The unexpected appearance of low-

solubility contaminants some distance from known sources, or sooner than would be expected from their solubility, led to examination of the possible involvement of non-aqueous, mobile colloids in contaminant transport³. Invoking colloids to explain such observations gave rise to three-phase models of contaminant transport (Fig. 2, overleaf). The results of Kersting *et al.* reinforce the need for such models. In their work, they use isotopic fingerprinting to demonstrate that Pu, an element with extremely low aqueous solubility (as low as 10^{-17} M, depending on

its oxidation state), was transported significant distances through a groundwater system and they argue that colloidal species were responsible.

Colloid-facilitated transport of contaminants has become a sort of Gordian knot for environmental scientists. Field studies have often been subject to sampling artefacts, such as colloid mobilization through excessive well pumping rates, and it has been difficult to reconcile field observations with theory and model simulations. (In 1988, a reviewer of a manuscript⁴, on which I was an author, implicating a colloidal intermediate in the scavenging of metals in marine systems, complained "The problem developing in the literature with colloids is that they are blamed or claimed for everything that can't be explained.") Since then, colloid-facilitated contaminant transport has gained broad acceptance. Nonetheless, few studies have unequivocally demonstrated its significance in the field.

Figure 2 compares two- and three-phase contaminant transport models. Figure 2a shows a low-solubility contaminant distributed between an aqueous phase and immobile aquifer solids (the macroparticles). Colloidal materials can increase the apparent solubility of low-solubility contaminants (Fig. 2b) if those contaminants strongly associate with the colloids and the colloids minimally interact with the stationary macroparticle phase. Because colloid groundwater concentrations are typically quite low, the contaminants most likely to be transported by colloidal materials are of extremely low solubility and strongly partition to mobile non-aqueous phase materials. In this respect Pu is an ideal candidate, others include pesticides (for instance DDT and dieldrin), polynuclear aromatic hydrocarbons, other light actinides (for example thorium) and many transition metals (such as cobalt).

Groundwater colloids originate from two sources⁵ through mobilization of existing colloid-sized (1 nm to 1 µm) materials in aquifer systems following chemical pertur-

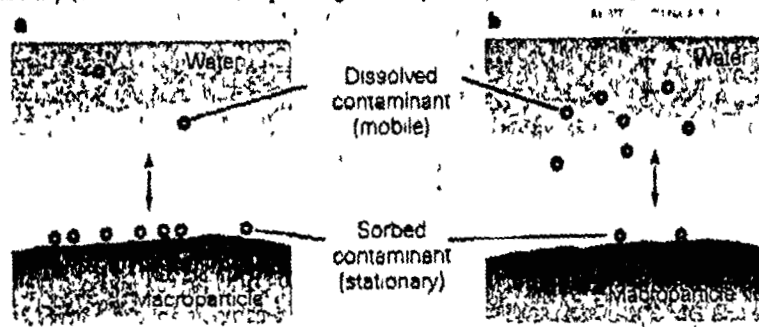


Figure 1 Contaminant transport in a simple two-phase groundwater system. a High sorption, and therefore low contaminant solubility. b Low sorption, high contaminant solubility. Macroparticles are the stationary components of a groundwater aquifer and include clays, metal oxides such as quartz, and particulate organic matter. The extent to which contaminant molecules are sorbed to macroparticles (by adsorption, surface precipitation or absorption) regulates the rate of contaminant transfer through groundwater systems for a given water velocity.

news and views



100 YEARS AGO

The native arithmetic of Murray Island, Torres Strait, is described by the Rev. A. E. Hunt in the latest *Journal* (New Series, vol. 1 Nos. 1 and 2) of the Anthropological Institute. The only native numerals are *netat* (one) and *neis* (two). Higher numbers would be described either by reduplication, as *neis-netat*, literally, two-one for three; *neis-neis*, or two-two for four, &c., or by reference to some part of the body. By the latter method a total of thirty-one could be counted. The counting commenced at the little finger of the left-hand, thence counting the digits, wrist, elbow, armpit, shoulder, hollow above the clavicle, thorax and thence in reverse order down the right arm, ending with little finger or right hand. This gives twenty-one. The toes are then resorted to, and these give ten more. Beyond this number the term *gaira* (many) would be used. English numerals are now in general use in the islands. From *Nature* 5 January 1899

50 YEARS AGO

Fertilized mouse ova have been cultivated *in vitro*, and their development filmed, by Friedrich-Freska and Kuhl, who used as medium a clot of guinea pig plasma and mouse embryo extract containing segments of Fallopian tube. Like Chang, I have been working on ovum culture with a view to transplantation of ova. Chang has used rabbits, with serum as a culture medium, I have chosen to use mice, as more readily available, and because (like most domestic animals) they have naked eggs. Seeking a medium readily prepared in large quantities, I have tried saline hen-egg extracts. The procedure adopted revealed an unanticipated difference between the viabilities of two-cell and later tubal stages, eight-cell ova survived and developed in culture, whereas two-cell ova did not. A few became blastocysts either completely separated from the zona, or spherical and still half enclosed in the split and distended membrane. A physiological difference between two-cell and eight-cell stages seems clearly established, the reason for the difference remains obscure. The result recalls a similar one of Chang's, namely, survival of morulae, but not two-cell ova, when transplanted into the rabbit uterus, though both survived when cultivated in serum. From *Nature* 1 January 1949

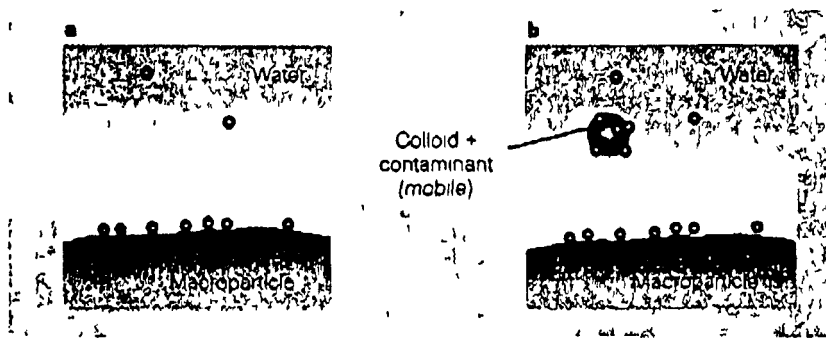


Figure 2 Comparison of generalized two- and three-phase groundwater systems. a, Two-phase, b, three-phase. The third phase in b is a colloid or microparticle shown here with contaminant molecules sorbed to it, thus making them mobile. Colloidal material is usually chemically similar to the stationary macroparticle phase.

bations or changes in flow velocity from pumping, and through *in situ* precipitation of supersaturated mineral phases. Colloids are removed from the aqueous phase by deposition on stationary macroparticles, it is the efficiency of deposition that regulates the facilitation of contaminant transport.

Kersting and colleagues' analysis¹ of colloids isolated from pumped ground water clearly identified the source of the Pu as a single underground nuclear test site, the test well and detonation site being 1.3 km apart. The elimination of other detonation cavities and contamination as the source of Pu makes it evident that the Pu has been transported through the ground water by some process.

As delineated by Ryan and Elimelech², however, three conditions must be met for defensible evidence that colloids have transported contaminants: first, colloids must be present, second, contaminants must associate with them, and third, the colloid-contaminant combination must move through the aquifer. The results of Kersting *et al.* qualitatively meet the first two conditions. But as the authors point out, the possibility of sampling artefacts meant that they could not quantify some of the parameters needed for supporting the detailed assessment of colloid-facilitated Pu transport in their study. That is, the third condition has not been rigorously met. Nevertheless their work clearly shows that a low solubility contaminant travelled some way from the source, perhaps at or near the local groundwater flow velocity (1–80 m yr⁻¹).

Has the Gordian knot been cut? No, I do not think so, although a good slice has been taken out of it. The fundamental difficulty remains the gap between field observations and expectations based on bench-scale experiments and theory. For example, according to classical filtration theory, colloid transport should be relatively limited (tens of metres or less under typical subsurface conditions). Advances in incorporating macroparticle chemical heterogeneity and site blockage into models have helped to narrow the gap, but it

nonetheless remains wide.

The trouble with most field studies is that the systems are difficult to manipulate, and are often too large and heterogeneous to characterize accurately. There is a great need to develop meso-scale experimental systems (several metres to more than ten metres) for the careful evaluation of the effects of system heterogeneity on colloid transport and the testing of methods for scaling up from the bench to the field.

Given that the work by Kersting *et al.* shows that Pu may be transported considerable distances through groundwater systems, can one conclude that the colloidal transport of actinides provides a significant exposure pathway from nuclear testing and waste sites? Not really. The very properties of compounds that make them good candidates for colloid facilitated transport—low solubility and high particle reactivity—limit the amount of contaminant that can be transported: colloids are both the means and the bottleneck. But we need to know more. T. H. Huxley³ had it that: It is the customary fate of new truths to begin as heresies and to end as superstitions [dogma]. In its evolution from heresy to dogma, colloid-facilitated contaminant transport has become a perceived truth, widely recognized, but rarely understood in detail. [7]

Bruce D. Hannayman is in the Environmental Science and Engineering Division, Colorado School of Mines, Golden, Colorado 80302, USA. e-mail: bhannayman@mines.edu

1. Kersting, A. B. *J. Colloid Interface Sci.* 197, 40–49 (1997).
2. Ruffin, I. & Leppard, G. G. *Environ. Sci. Technol.* 1997, 31, 1275–1281 (1997).
3. M. C. G. Ellis, J. P. Zedler, J. M. J. *Environ. Sci. Technol.* 23, 401–402 (1989).
4. H. J. G. J. M. J. & N. H. J. *J. Environ. Sci. Technol.* 1997, 31, 1275–1281 (1997).
5. Ruffin, I. N. & Leppard, G. G. *Environ. Sci. Technol.* 1997, 31, 1275–1281 (1997).
6. Ruffin, I. N. & Leppard, G. G. *Environ. Sci. Technol.* 1997, 31, 1275–1281 (1997).
7. M. C. G. Ellis, J. P. Zedler, J. M. J. *Environ. Sci. Technol.* 23, 401–402 (1989).
8. Ruffin, I. N. & Leppard, G. G. *Environ. Sci. Technol.* 1997, 31, 1275–1281 (1997).
9. Huxley, T. H. *Environ. Sci. Technol.* 1997, 31, 1275–1281 (1997).

13/13